Particle surface engineering effect on the mechanical, optical and photoluminescent properties of ZnO/vinyl-ester resin nanocomposites

Zhanhu Guo,*[a] Suying Wei,[b] Brian Shedd,[a] Roberto Scaffaro,[a] Tony Pereira[a] and H. Thomas Hahn*[a]

Received 13th September 2006, Accepted 22nd November 2006
First published as an Advance Article on the web 1st December 2006
DOI: 10.1039/b613286c

Zinc oxide (ZnO) nanoparticles functionalized with a bi-functional coupling agent methacryloxypropyl-trimethoxysilane (MPS) were used to fabricate a vinyl-ester resin polymeric nanocomposite, which shows an improved interfacial interaction between the particle and matrix. As a result, in comparison to the unmodified particle-filled nanocomposites, the functionalized particle-filled composites possessed higher resistance to thermal degradation, and demonstrated improved UV shielding and enhanced photoluminescent properties. The more uniform particle dispersion, passivation of the particle surface with MPS and increased oxygen vacancies were justified to contribute to the increased thermal stability and the enhanced photoluminescent properties. Significant tensile strength improvement was closely related to the observed uniform particle distribution and the intimate interfacial interaction through the strong chemical bonding.

1. Introduction

Zinc oxide (ZnO) is traditionally known as a wide band-gap (3.36 eV) semiconductor with an exciton binding energy (60 meV) larger than its thermal energy which ensures an efficient ultraviolet-blue emission (26 meV) at room temperature, thus yielding a wide range of potential applications in various devices such as UV lasers,[1] solar cells,[2–4] high-sensitivity chemical gas[5] or volatile organic compound[6] sensors, and DNA sequence[7] sensors. Polymer nanocomposites with nanoparticles (NPs) incorporated into the polymeric matrices have attracted much interest due to their high homogeneity, flexible processability, and tunable physical (mechanical, magnetic, electric and electronic) properties.[8–18] The reported methods for incorporating inorganic nanoparticles into polymeric matrices include *ex-situ* methods, *i.e.* dispersion of the synthesized nanoparticles into polymeric solution, or *in-situ* monomer polymerization methods in the presence of the nanoparticles.[15,19,20] The interactions between the polymer matrix and the nanoparticles for the *ex-situ*-formed composites are normally steric interaction forces, van der Waals forces, or Lewis acid–base interactions; however, the *in-situ* synthesis methods can create strong chemical bonding within the nanocomposites, potentially producing a more-stable and higher-quality nanocomposite.[21–23] Nevertheless, the former has the advantage of being able to utilize a large variety of nanoparticles that have recently become available.

The interfacial interactions between the nanoparticles and polymer matrix play a crucial role in determining the quality and properties of the nanocomposite. Poor bonding between the particles and the polymer matrix may also introduce artificial defects such as voids, which consequently have a deleterious effect on the mechanical properties. Thus, surface functionalization of the nanoparticles with a surfactant or a coupling agent is important not only to stabilize the nanoparticles[24] during processing but also to render them compatible with the polymer matrix.

Vinyl-ester resin is chosen as a polymer matrix in the present research because it is widely used as a structural polymer having good resistance to moisture and chemicals, and good mechanical properties. Thus the resultant composites can be used in harsh environments. The photoluminescent and special electronic properties of zinc oxide provide potential applications of the obtained composite in the biological areas such as photo-enhanced imaging[7] and site-specific molecule targeting at the polymeric functional groups,[25] and in optical-electronic device fabrication.

The present paper investigates the effect of a bi-functional surfactant, methacryloxypropyl-trimethoxysilane (MPS), on the processing and properties of a nanocomposite consisting of a vinyl-ester resin reinforced with zinc oxide nanoparticles. FT-IR, TGA and XPS analyses indicate that MPS is covalently bound onto the nanoparticle surface. The particle functionalization and loading have significant effects on the optical, photoluminescent and mechanical properties (tensile strength and Young's modulus) of the fabricated nanocomposites.

2. Experimental

Materials

The polymeric matrix used is a vinyl-ester (VE) resin, Derakane momentum 411-350 (manufactured by the Dow Chemical Company), which is a mixture of 55 wt% vinyl-ester with an average molecule weight of 970 g mol^{-1} and 45 wt% styrene monomer. Zinc oxide (ZnO) nanoparticles having an average diameter of 60 nm (provided by the manufacturer *via* TEM measurements) were purchased from Nanophase Technologies. Trigonox 239-A (curing catalyst or initiator,

[a]*Multifunctional Composites Lab (MCL), Mechanical & Aerospace Engineering and Materials Science & Engineering Department, University of California, Los Angeles, CA 90095, USA*
[b]*Department of Chemistry, Louisiana State University, Baton Rouge, LA 70803, USA*

an organic peroxide, liquid) was purchased from Akzo Nobel Chemicals. Cobalt naphthenate (CoNap, OM Group, Inc.) was used as a room-temperature promoter (accelerator). Methacryloxypropyl-trimethoxysilane (MPS), tetrahydrofuran (THF, anhydrous) and ethanol (anhydrous) were purchased from Sigma-Aldrich Chemical Company. All the chemicals were used as-received without further treatment.

Surface functionalization of ZnO nanoparticles

The nanoparticle functionalization follows the procedures similar to those used for alumina nanoparticles[26] and is described briefly here. ZnO nanoparticles weighing 6.822 g (83.8 mmol) were added into a mixture of 4 g MPS and 50 ml THF. The resulting colloidal suspension was ultrasonically (Branson 1510) stirred for one hour and precipitated at room temperature. The precipitated nanoparticles were rinsed with THF to remove excessive MPS and dried completely in a vacuum oven at room temperature to remove the solvent.

Nanocomposite fabrication

The as-received ZnO nanoparticles and MPS-functionalized ZnO nanoparticles (specific weight percentage) were dispersed into 30 ml vinyl-ester (VE) in a container. The dispersion was carried out in an ice-water ultrasonic bath for about one hour. The nanoparticle/resin suspension was placed into a vacuum oven at 85 °C for 15 min to remove gases. The suspension was then ultrasonically stirred again in an ice-water ultrasonic bath until the temperature cooled down to room temperature. Then the catalyst (2.0 wt%) was added into the nanoparticle/resin suspension. After being stirred for 2 min, the suspension was mixed with 0.3 wt% of promoter. The final viscous suspension was poured into various silicone rubber molds. The specimens thus prepared were cured at room temperature for 30 min followed by post-curing at 85 °C for one hour under ambient pressure. They were finally cooled down to room temperature in an air-circulating oven.

Characterization

A Fourier transform infra-red (FT-IR) spectrometer (Jasco, FT-IR 420) in transmission mode under dry nitrogen flow (10 cm^3 min^{-1}) was used to test the physicochemical interactions between MPS and the ZnO nanoparticles. The liquid MPS was mixed with powder KBr, ground and compressed into a pellet. Its spectrum was recorded as a reference to be compared with that of the MPS-functionalized ZnO nanoparticles. The chemical bonding between MPS and the nanoparticle surface was further characterized using an Axis 165 X-ray Photoelectron Spectrometer (XPS; Kratos Analytical) using a monochromatized Al Kα (1486.6 eV) X-ray source with a power of 150 W. Survey and high-resolution spectra were obtained using a pass energy of 40 eV. Quantification of the data was carried out using the curve-fitting program provided by the instrument vendor. The curve-fitting was performed using a sum of the Gaussian–Lorentzian profile peak shapes after subtraction of a linear background.[10] Thermogravimetric analysis (TGA, Perkin Elmer) was conducted on the as-received and MPS-treated ZnO nanoparticles from 25 to 600 °C with an argon flow rate of 50 cm^3 min^{-1} and a heating rate of 10 °C min^{-1}. Thermal degradation of the nanocomposites with different nanoparticle loadings was studied by TGA with procedures similar to nanoparticles.

Atomic force microscopy (AFM) (Digital, Instruments, Veeco Metrology Company, Santa Barbara, CA) with the instrument in tapping mode was utilized to characterize the morphology (size and shape) of the as-received and MPS-treated ZnO nanoparticles. The probes used were TappingMode etched silicon probes with resonant frequency about 300 kHz and spring constant of around 40 N m^{-1}. Specimens were prepared by dispersing the nanoparticles in ethanol under ultrasonic stirring, dropping some of the solution onto a glass slide, and evaporating the solvent naturally. The dispersion quality of the nanoparticles within the vinyl-ester resin matrix was investigated by AFM and SEM (scanning electron microscope, JEOL field emission scanning electron microscope, JSM-6700F) on polished cross-sections. The SEM specimens were prepared by sputter coating a thin gold layer about 3 nm thick.

Optical absorption of the nanocomposites was measured in a UV-VIS-NIR scanning spectrophotometer (Mode: UV-310PC). The steady-state photoluminescent emission property was measured in an Ocean Optics system with a home-made lamp using an inorganic light emitting diode (LED) with an excitation wavelength of 365 nm. A long wavelength pass filter was used to cut off the emission lower than 380 nm to remove the reflection effect. Optical absorption and photon-excited luminescence were recorded in a nanocomposite thin film with a thickness of about 300 μm. Specimens were prepared by polishing the composites first with 4000 grit sand paper and then with 50 nm alumina particles. All experiments were conducted at room temperature.

The tensile strength and Young's modulus of the fabricated nanocomposites were evaluated by microtensile tests following the American Society for Testing and Materials Standard (ASTM, Standard D 1708-02a, 2005) using an Instron 5544 testing machine. A crosshead speed of 0.15 mm min^{-1} was used and strain (mm mm^{-1}) was calculated by dividing the crosshead displacement (mm) by the gage length (mm). The fracture surfaces were examined on a bright-field optical microscope (OM, Olympus BX41).

3. Results and discussion

Thermogravimetric analyses of the as-received and MPS-treated ZnO nanoparticles show the existence of moisture by physical adsorption and hydroxy groups by chemical bonding in Fig. 1. With the temperature lower than A and B, the weight loss is from evaporation of the physically adsorbed moisture in both the as-received nanoparticles and MPS-treated nanoparticles. Beyond A and B, dehydration of the chemically adsorbed water (Zn–OH) in the as-received nanoparticles and of the hydrolyzed functional group (Si–OH) in the MPS-treated nanoparticles leads to weight losses. After a TGA run, there was no color change in the as-received nanoparticles. However, the MPS-treated nanoparticles turned from white to dark grey, indicating the existence and partial decomposition of the surfactant. Further information on the functional

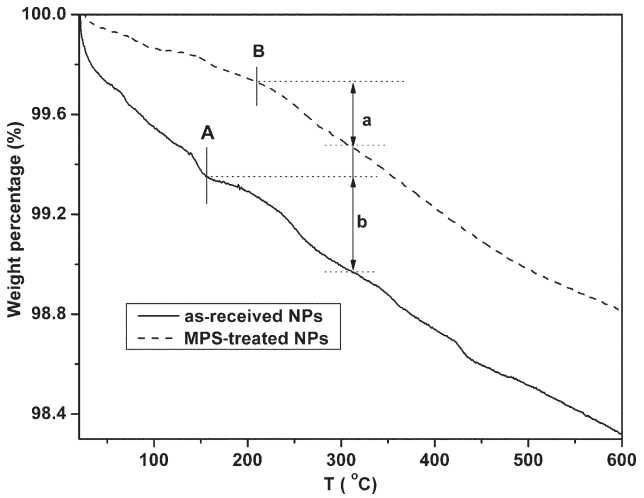

Fig. 1 Weight changes in TGA of as-received and MPS-treated ZnO nanoparticles.

linkage of MPS to the zinc oxide particle surface can be extracted from the chemical dehydration data shown in the TGA graphs of Fig. 1. The relative weight losses arising from the chemical dehydration of the MPS-treated and as-received nanoparticles as represented by 'a' and 'b' in Fig. 1 show that the MPS-treated nanoparticles lost less weight (0.0026) than the as-received nanoparticles (0.0382). Considering partial weight loss from the decomposition of MPS and the smaller weight loss in the MPS-treated ZnO nanoparticles, it is reasonable to deduce that more than one hydrolyzed functional group (Si–OH) in one MPS molecule reacted with the chemically adsorbed –OH on the nanoparticle surface, which is consistent with the report for the MPS-grafted silica gel.[27]

FT-IR spectra of the as-received ZnO nanoparticles, pure MPS and MPS-treated ZnO nanoparticles are shown in Fig. 2. In the MPS spectrum, the bands at 1720, 1640 and 1167 cm^{-1} belong to C=O, C=C and C–O vibrations, respectively. The peak at 903 cm^{-1} originates from the Si–O stretching of SiOH groups due to the partial hydrolysis of MPS; while the intense

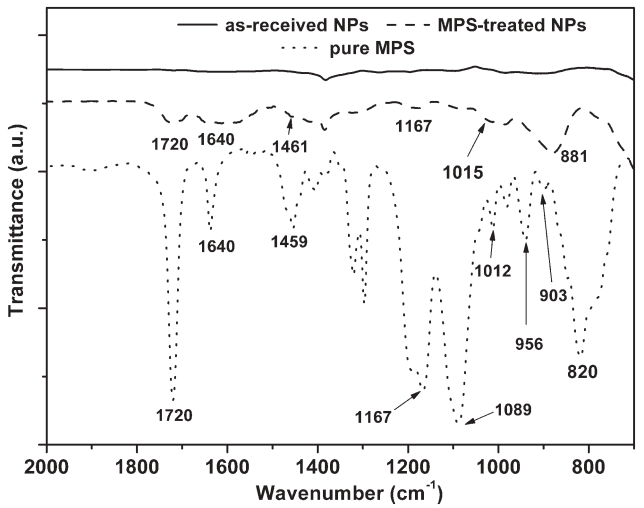

Fig. 2 FT-IR spectra of the as-received nanoparticles, pure MPS and MPS-treated ZnO nanoparticles.

and characteristic band at 820 cm^{-1} originates from the symmetric stretch of Si–O–CH_3. In contrast with the absence of any characteristic bands of MPS in the as-received nanoparticles, the spectrum of the MPS-treated ZnO nanoparticles shows the characteristic peaks (C=O, C=C and C–O) of MPS, indicating the presence of MPS after functionalization. The observed relative broader and wider spectral bands of MPS bound onto the nanoparticles could be due to the particle effect, which has been observed in the gels containing alumina/zirconium-oxide modified by silica[28] and ZnO nanoparticles functionalized with silicate.[29] In addition, the intensity ratio of two peaks in FT-IR do not necessarily relate to the ratio of two functional groups. In other words, the intensity ratio is a multi-factor-dependent parameter such as the existing environmental media, which could have a dramatic effect on some specific peak (functional group). For example, dodecylphosphonic acid (DDP, a surfactant) attached to the magnetic nanoparticles could even reverse the ratio of certain peaks as compared with the pure surfactant DDP.[30] The peak at 1015 cm^{-1} in the functionalized nanoparticles is attributed to Si–O–Si, consistent with that reported in the standard FT-IR spectra.[31] The disappearance of the peak at 820 cm^{-1}, characteristic of Si–O–CH_3, and the presence of other peaks indicate the complete reaction between the hydrolyzed ZnO nanoparticles and the MPS. The new peak around 881 cm^{-1} could be from the formed Si–O–Zn bond.

As a powerful surface analysis tool, XPS is able to provide information on the oxidation state of each component in the sample as well as the composition of the sample surface. Functionalization of the ZnO nanoparticles is happening on the particle surface layer, thus it makes XPS more suitable for investigation and monitoring the surface functionalization. High-resolution region spectra of the key elemental composition provide detailed individual component information such as chemical shift and intensity changes, indicating changes of bonding among individual elements; while survey spectra of the samples can only give a quick idea of how the composition is changing and to what degree it changes. In this work, the surface of the ZnO nanoparticles is functionalized with MPS through covalent bonding between zinc, oxygen, and silicon. Hence, the electronic states of both zinc and oxygen are altered as evidenced in Fig. 3. There are two sets of zinc peaks in both the as-received ZnO nanoparticles and the MPS-modified ZnO nanoparticles. The Zn 2p peaks at binding energies of 1019.4 eV (Zn $2p_{3/2}$) and 1042.3 eV (Zn $2p_{1/2}$) are from the $Zn(OH)_2$ molecular environment, while the Zn 2p peaks at binding energies of 1021.7 eV (Zn $2p_{3/2}$) and 1044.7 eV (Zn $2p_{1/2}$) are attributed to the ZnO molecular environment.[32] Meanwhile, O 1s has shifted to a lower binding energy region, for more electron-rich oxygen components are incorporated after the MPS surface modification of the ZnO nanoparticles. Abboud *et al.*[33] reported that the hydroxy groups on the nanoparticle surface react with MPS at temperatures between 400 and 1100 °C. However, irradiation with ultrasound causes the formation, growth and implosive collapse of bubbles, generating hot spots of thousands of Kelvin (*ca.* 5200 K)[34] which have been used in the fabrication of various nanoparticles.[34–36] The low-temperature nanoparticle surface functionalization that happened in the present study is from the

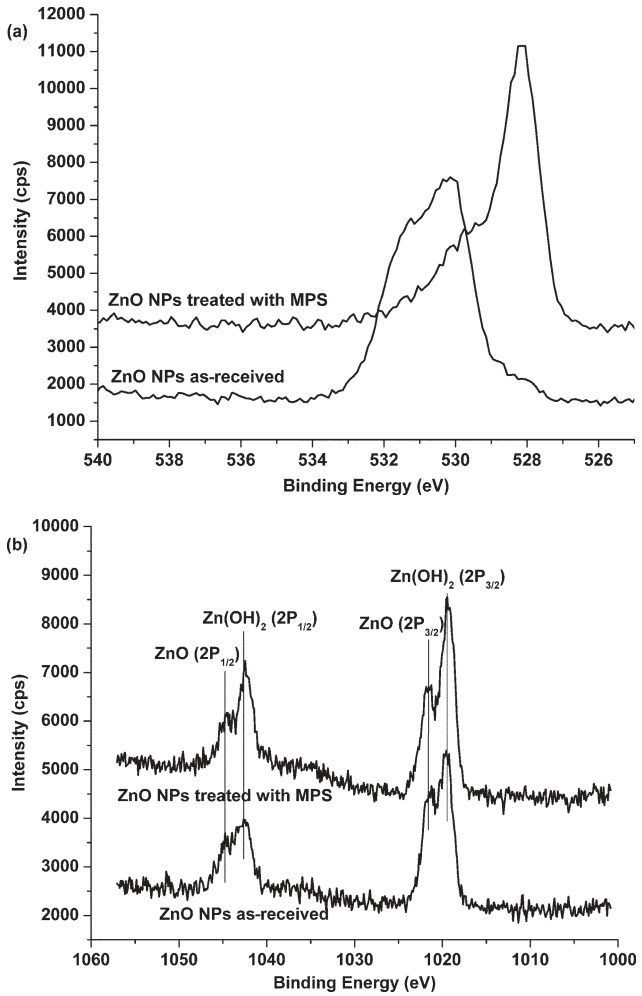

Fig. 3 (a) High-resolution O 1s XPS spectra of ZnO NPS and ZnO NPS treated with MPS; and (b) high-resolution Zn 2p XPS spectra of ZnO NPS and ZnO NPS treated with MPS.

ultrasonic stirring. It is noted that ultrasonication is also necessary for the nanoparticle dispersion.

Fig. 4(a) and (b) show the AFM phase images under tapping mode of the as-received ZnO nanoparticles and MPS-treated

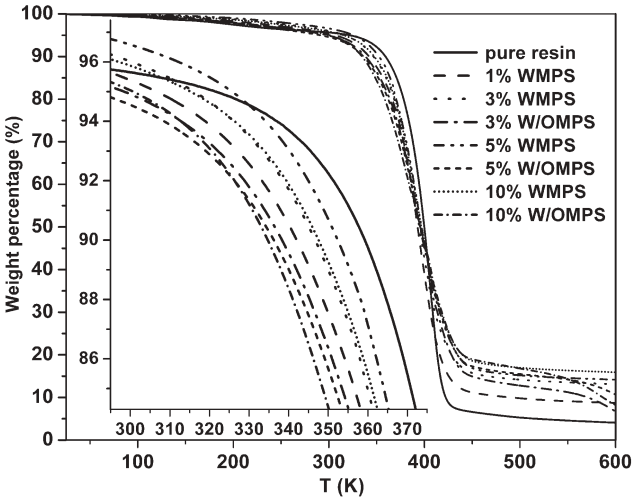

Fig. 5 Weight changes in TGA of as-received and MPS-treated nanocomposites at different particle loadings (inset shows the enlarged graph near the decomposition point).

ZnO nanoparticles. The observed dimensions are about 75 nm for the former and 87 nm for the latter. The dimensions are larger than the reported average size of 60 nm, which may be due to the convolution of the AFM tip shape and the real topography of the nanoparticles similar to that observed in iron oxide nanoparticles.[37]

Fig. 5 shows thermogravimetric profiles of nanocomposites with different particle loadings (0, 1, 3, 5, and 10 wt%). The thermal stability of the nanocomposites decreases slightly with the addition of nanoparticles. This is consistent with the early observation on the unwetted alumina nanoparticle-filled PMMA nanocomposites,[38] layered silicate-filled polyurethane nanocomposites,[39] and ZnO particle-filled polyacrylate[40] or dianhydride-4,4′-diaminodiphenyl ether[41] nanocomposites. However, the MPS treatment reduces the nanoparticle-induced degradation of the nanocomposites, which is consistent with the recently reported observation on silica-filled polystyrene nanocomposite[42] and clay-filled diglycidylether (SC-15) epoxy nanocomposite.[43] The beneficial nature of MPS treatment can be explained by the MPS-induced physicochemical interaction

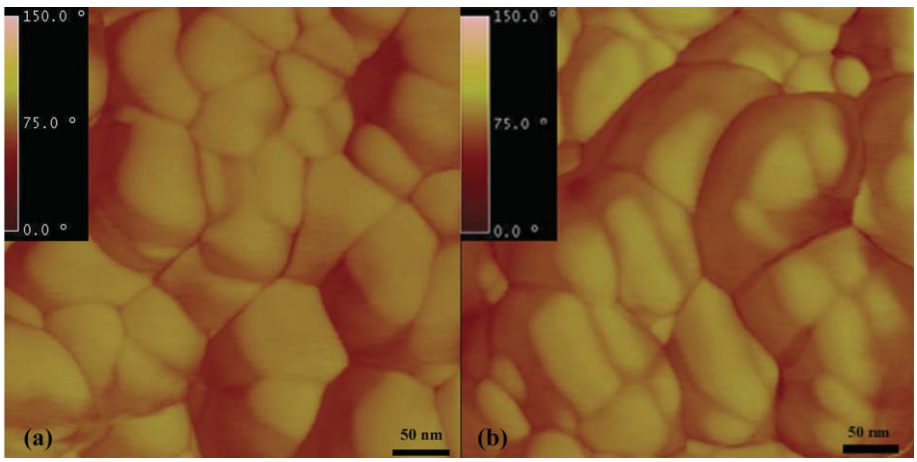

Fig. 4 AFM images of the (a) as-received ZnO and (b) MPS-treated ZnO nanoparticles.

differences between the particle and the matrix. As-received nanoparticles are non-wetting and have poor chemical bonding with the polymer matrix. This weak linkage and possible air voids lead to the reduction in thermal stability. On the other hand, the MPS-treated nanoparticles form a chemical bond with the polymer molecules. Thus the MPS-treated ZnO nanoparticle-filled vinyl-ester resin nanocomposite has improved thermally stable behavior as compared with the as-received nanoparticle-filled nanocomposite. Furthermore, it was reported that metallic compounds could serve as catalysts to degrade the polymer matrix with an inferior thermal stability.[41,44–46] The presence of the as-received ZnO nanoparticle in the nanocomposites may facilitate the thermal degradation of the vinyl-ester resin by serving as a catalyst. However, the existence of a thin interfacial layer through the bridging effect of MPS prevents the intimate contact of the ZnO nanoparticle with the vinyl-ester resin by passivating the particle surface and thus improves the thermal stability of the nanocomposites.

Fig. 6 shows the UV/vis absorption spectra of the as-received and MPS-treated ZnO/vinyl-ester nanocomposites at different particle loadings. At higher particle loadings, a big jump in absorption is noticed at about 358 nm. The peak shifts from 372 nm for the MPS-treated ZnO nanocomposite to 382 nm for the as-received nanocomposite. Here, the big jump and the shift toward a larger wavelength in the as-received nanocomposite is attributed to the agglomeration of ZnO nanoparticles.[47–51] The observed absorption is around the UV region indicating that this type of composite could be used as a paint-on or spray-on coating to shield against UV light.

Fig. 7 depicts the concentration dependence of the room-temperature excitation luminescent emission spectra of the nanocomposites. No luminescence was observed in the neat vinyl-ester resin as expected. However, strong luminescence was observed in the composites filled with even 1 wt% ZnO nanoparticles. The concentration has little effect on the frequency (wavelength) spectrum of the emitted photons because the particle size is too large to exhibit a quantum

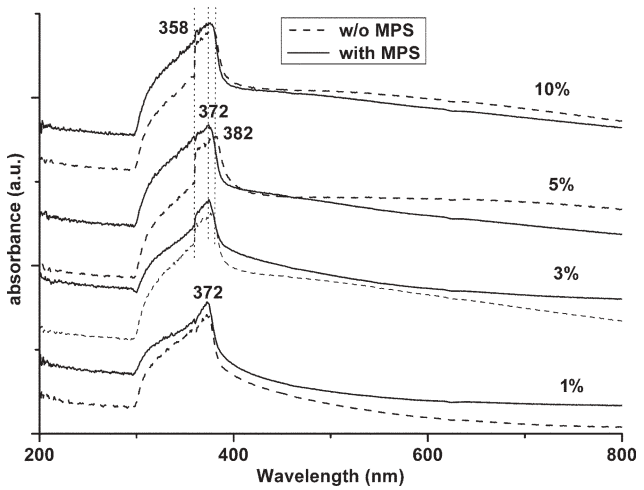

Fig. 6 Optical absorption spectra of as-received and MPS-treated nanocomposites at different particle loadings.

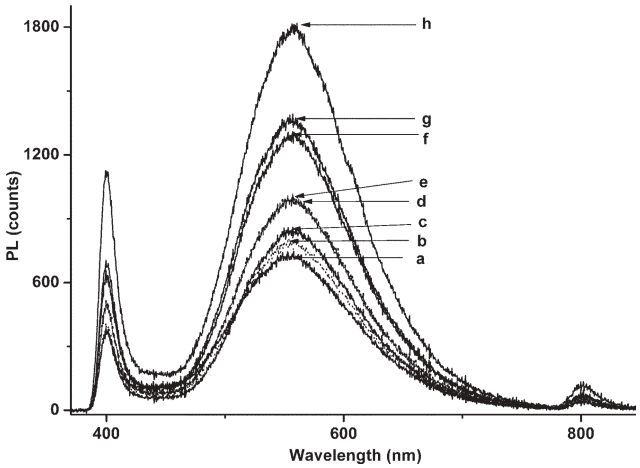

Fig. 7 Luminescence spectra of nanocomposites with various particle loadings: (a) 1 wt% as-received, (b) 1 wt% MPS-treated, (c) 3 wt% as-received, (d) 5 wt% as-received, (e) 3 wt% MPS-treated, (f) 5 wt% MPS-treated, (g) 10 wt% as-received, and (h) 10 wt% MPS-treated ZnO nanoparticles.

size effect;[52,53] however, it does increase the luminescence quantum yield, which was reflected in the intensity increase of the photoluminescence spectra as shown in Fig. 7. It is reported that the characteristic luminescent spectrum of ZnO exhibits two maxima: around 380 nm (near-UV emission) and 500 nm (green emission), respectively. The former is attributed to the exciton band (band-gap fluorescence caused by a transition from the lower edge of the conduction band to the upper edge of the valence band) recombination.[54] The latter is attributed to the density of singly ionized oxygen vacancies.[55–57] Disappearance of the spectrum peak at 380 nm in Fig. 7 is a result of the filter used in our experiment to prevent the reflection of the light from the light source. In these experiments, visible light (557 nm) was detected from an excitation source of 365 nm and the luminescent intensity was observed to depend strongly on the concentration of the nanoparticles, with the intensity increasing with increasing particle loading, which is consistent with the observation that the emission intensity is dependent on the amount of emitting nanoparticles.[48,52] Furthermore, the MPS-treated nanocomposites demonstrate a higher luminescence compared to the as-received nanocomposites.

In order to interpret the aforementioned optical and photoluminescent phenomena, the microstructure of the nanocomposites was studied by AFM. Fig. 8 shows the typical AFM tapping mode phase images of polished cross-sections of the nanocomposites containing (a) as-received and (b) MPS-treated ZnO nanoparticles, both with a particle loading of 10 wt%. The nanoparticle dispersion quality in the polymeric matrix is better with MPS-treated ZnO nanoparticles. In addition, the AFM contrast shows an intermediate phase in the composites containing MPS-treated nanoparticles indicating strong chemical bonding between the nanoparticle and polymer matrix. It has been reported that ZnO nanoparticles stabilized with different surfactants give different defect-induced visible emission intensities, which is attributed to oxygen vacancy content in the ZnO nanoparticle.[52,57,58]

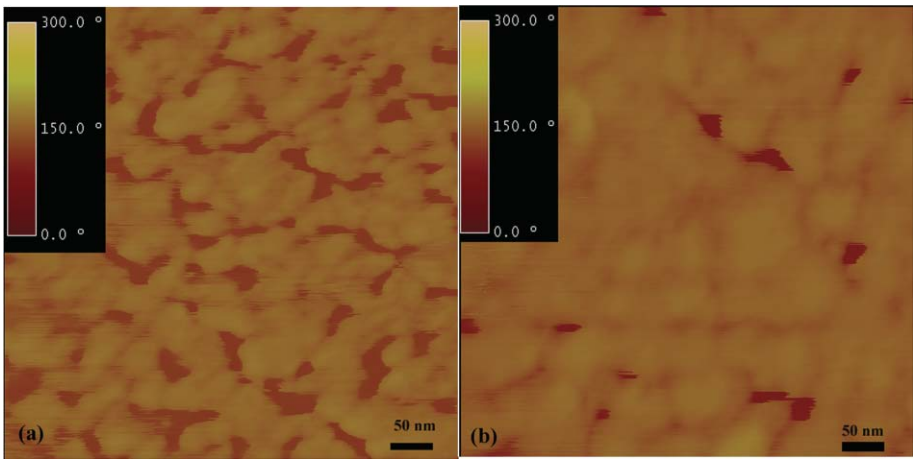

Fig. 8 AFM phase images of (a) as-received and (b) MPS-treated nanocomposites (10 wt%).

Strong attachment of oxygen ions in the amphoteric surfactant lauryl dimethylaminoacetic acid betaine [LDA, $(CH_3(CH_2)_{11}N^+(CH_3)CH_2COO^-)$] to the nanoparticle surface passivates the oxygen vacancies, decreasing the emission intensity with the increasing surfactant concentration.[52] In the present study, the MPS which is chemically bound onto the ZnO nanoparticle surface (Zn–O–Si) could increase the oxygen vacancy density as compared with the hydrolyzed ZnO (Zn–O–H). This could be a reason for the increased photoluminescence intensity observed. This passivation can also help explain the improved thermal stability in the MPS-treated nanoparticle-filled vinyl-ester resin nanocomposite over that containing the as-received nanoparticles.

The mechanical properties (tensile modulus and strength) of the neat resin and nanocomposites were measured by microtensile tests. Fig. 9 shows the tensile strength (the maximum stress) and Young's modulus as a function of nanoparticle loading. The Young's modulus is seen to increase with the particle loading regardless of particle functionalization. However, the tensile strength decreases when as-received nanoparticles are introduced into the resin. In contrast, the addition of MPS-treated nanoparticles enhances the tensile strength with increasing particle loading, which is consistent with the results reported recently on alumina-filled polyethylene nanocomposites[59] and alumina-filled VE resin nanocomposites.[26]

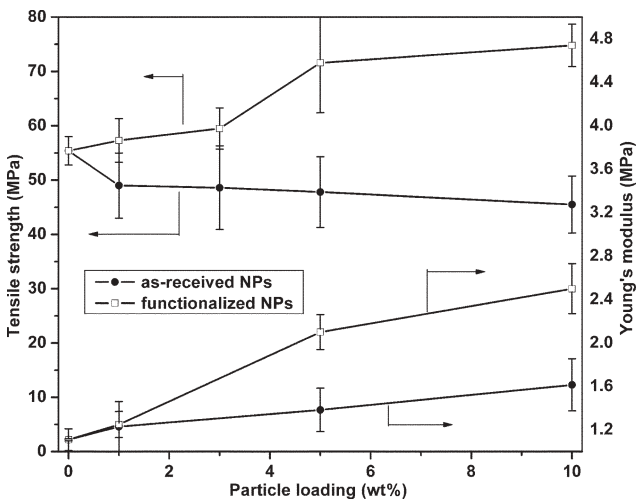

Fig. 9 Tensile strength and Young's modulus as a function of nanoparticle loading.

Typical fracture surfaces of the nanocomposites filled with as-received and MPS-treated nanoparticles at different particle loadings (1 and 10 wt%) are shown in Fig. 10. Our previous study showed that the neat resin revealed a fracture surface typical of a brittle polymer, large smooth areas combined with river patterns.[26] However, the nanocomposites show rougher fracture surfaces with many crack initiation regions indicating an increased toughness, which originate from the nanoparticles. The granular regions in the fracture surface become smaller and smaller with increasing particle loading in both as-received and MPS-treated nanocomposites. The same type of fracture surfaces were also reported in the clay-filled epoxy nanocomposite[43] and polyamide-6 nanocomposite.[60] This micron-rough structure may be attributed to the matrix shear yielding or local polymer deformation as the nanoparticles serve as crack stoppers.[18]

In general, the presence of micron-size hard particles introduces stress concentrations, rendering the resulting composite more brittle than the matrix polymer itself. When nano-sized particles are used, however, both modulus and strength could be improved if the nanoparticles were uniformly distributed and the interfacial bonding was strong. In fact, the increase in modulus is more than predicted by the rule of mixtures. This may be explained by the formation of an interphase which is stiffer than the matrix.[21] Such an interphase will also reduce the stress concentration in the matrix, thereby improving the composite strength, consistent with the carboxylic acid- and amide-functionalized carbon nanotube-reinforced nylon-6 nanocomposites.[61] For the same particle loading, the fraction of interphase will increase with decreasing particle size. However, agglomerated nanoparticles will act like larger particles, thereby reducing strength, Fig. 11(a). The MPS treatment improves particle dispersion, Fig. 11(b), and led to increased strength.

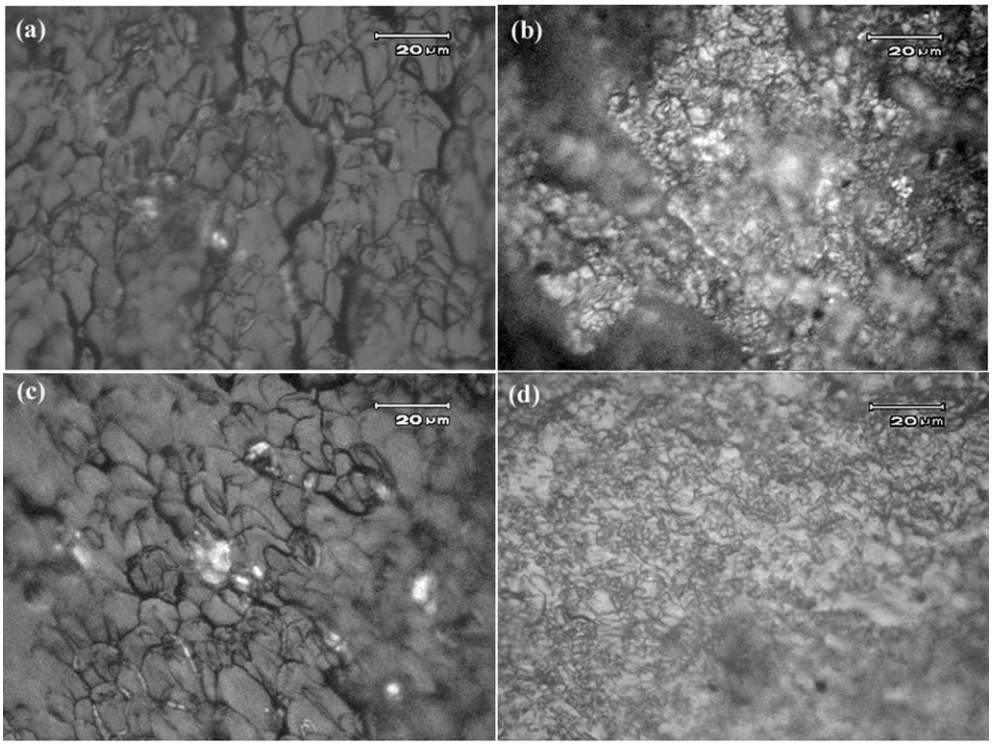

Fig. 10 Bright-field optical micrographs of fracture surfaces of nanocomposites with as-received particle loadings of (a) 1 wt%, and (b) 10 wt%; and with MPS-treated particle loadings of (c) 1 wt%, and (d) 10 wt%, respectively.

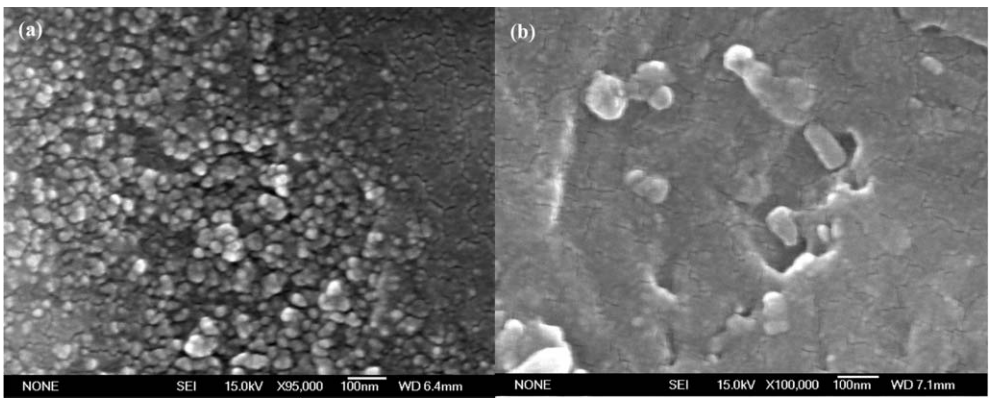

Fig. 11 SEM micrographs of nanocomposites after polishing with a 10 wt% particle loading (a) as-received and (b) MPS-treated ZnO nanoparticle, respectively.

4. Summary

The optical and mechanical properties of vinyl-ester resin nanocomposites reinforced with ZnO nanoparticles can be improved by a facile particle surface functionalization. The existence of MPS between the particle and the polymer matrix results in an interphase which promotes a more uniform particle distribution and a gradual property change. The MPS treatment improves not only UV shielding and photoluminescence but also modulus and strength. Passivation of the ZnO nanoparticle surface with MPS also made the composites more resistant to thermal degradation. The larger surface area available with nanoparticles and the increased oxygen vacancy resulting from MPS treatment leads to the enhancement of the UV shielding and photoluminescence. The presence of an interphase between the nanoparticles and the polymer matrix improves both modulus and strength significantly.

Acknowledgements

The present paper is based on work supported by the Air Force Office of Scientific Research through AFOSR Grant FA9550-05-1-0138 with Dr B. Les Lee as the Program Manager. The FT-IR spectroscopy, TGA and SEM were done in the MCTP lab which is supported by the NSF IGERT Materials Creation Training Program under Grant DGE-0114443.

References

1 M. H. Huang, S. Mao, H. Feick, H. Yan, Y. Wu, H. Kind, E. Weber, R. Russo and P. Yang, *Science*, 2001, **292**, 1897.
2 H. Rensmo, K. Keis, H. Lindstroem, S. Soedergren, A. Solbrand, A. Hagfeldt, S. E. Lindquist, L. N. Wang and M. Muhammed, *J. Phys. Chem. B*, 1997, **101**, 2598.
3 J. Bandara and H. C. Weerasinghe, *Sol. Energy Mater. Sol. Cells*, 2005, **88**, 341.
4 E. Hosono, S. Fujihara, I. Honma and H. Zhou, *Adv. Mater.*, 2005, **17**, 2091.
5 H. Tang, M. Yan, X. Ma, H. Zhang, M. Wang and D. Yang, *Sens. Actuators, B*, 2006, **113**, 324.
6 G. G. Huang, C. Wang, H. Tang, Y. Huang and J. Yang, *Anal. Chem.*, 2006, **78**, 2397.
7 N. Kumar, A. Dorfman and J. Hahm, *Nanotechnology*, 2006, **17**, 2875.
8 C. Castro, J. Ramos, A. Millan, J. Gonzalez-Calbet and F. Palacio, *Chem. Mater.*, 2000, **12**, 3681.
9 M. K. Corbierre, N. S. Cameron, M. Sutton, S. Mochrie, L. Lurio, A. Ruehm and R. Lennox, *J. Am. Chem. Soc.*, 2001, **123**, 10 411.
10 S. Wei, B. Vaidya, A. B. Patel, S. A. Soper and R. L. McCarley, *J. Phys. Chem. B*, 2005, **109**, 16 988.
11 V. Yong and H. T. Hahn, *Nanotechnology*, 2004, **15**, 1338.
12 J. Mack, L. Viculis, A. Ali, R. Luoh, G. Yang, H. T. Hahn, F. Ko and R. B. Kaner, *Adv. Mater.*, 2005, **17**, 77.
13 G. Sandi, H. Joachin, R. Kizilel, S. Seifert and K. A. Carrado, *Chem. Mater.*, 2003, **15**, 838.
14 G. Sandi, R. Kizilel, K. A. Carrado, R. Fernandez-Saavedra and N. Castagnola, *Electrochim. Acta*, 2005, **50**, 3891.
15 Z. Guo, L. L. Henry, V. Palshin and E. J. Podlaha, *J. Mater. Chem.*, 2006, **16**, 1772.
16 J. M. Brown, D. P. Anderson, R. S. Justice, K. Lafdi, M. Belfor, K. L. Strong and D. W. Schaefer, *Polymer*, 2005, **46**, 10 854.
17 Y. Chen, L. Sun, O. Chiparus, I. Negulescu, V. Yachmenev and M. Warnock, *J. Polym. Environ.*, 2005, **13**, 107.
18 B. Wetzel, F. Haupert and M. Q. Zhang, *Compos. Sci. Technol.*, 2003, **63**, 2055.
19 E. Marutani, S. Yamamoto, T. Ninjbadgar, Y. Tsujii, T. Fukuda and M. Takano, *Polymer*, 2004, **45**, 2231.
20 S. Yu and G. Chow, *J. Mater. Chem.*, 2004, **14**, 2781.
21 C. Sanchez and F. Ribot, *New J. Chem.*, 1994, **18**, 1007.
22 J. Patrick and C. Sanchez, *J. Mater. Chem.*, 1996, **6**, 511.
23 F. Mammeri, E. L. Bourhis, L. Rozes and C. Sanchez, *J. Mater. Chem.*, 2005, **15**, 3787.
24 R. Shenhar, T. B. Norsten and W. M. Rotello, *Adv. Mater.*, 2005, **17**, 657.
25 N. Kohli, R. M. Worden and I. Lee, *Chem. Commun.*, 2005, 316.
26 Z. Guo, T. Pereira, O. Choi, Y. Wang and H. T. Hahn, *J. Mater. Chem.*, 2006, **16**, 2800.
27 J. W. De Haan, H. M. Van den Bogaert, J. J. Ponjee and L. J. M. Van de Ven, *J. Colloid Interface Sci.*, 1986, **110**, 591.
28 Y. Ade, N. Sugimoto and T. Misono, *J. Non-Cryst. Solids*, 1989, **108**, 150.
29 R. Hong, T. Pan, J. Qian and H. Li, *Chem. Eng. J. (Amsterdam, Neth.)*, 2006, **119**, 71.
30 Y. Sahoo, H. Pizem, T. Fried, D. Golodnitsky, L. Burstein, C. N. Sukenik and G. Markovich, *Langmuir*, 2001, **17**, 7907.
31 *Aldrich Library of FT-IR Spectra*, Aldrich Chemical Co., Milwaukee, WI, 2nd edn, 1997.
32 S. Surviliene, A. Cesuniene and D. Bucinskiene, *Chemija*, 2002, **13**, 214.
33 M. Abboud, M. Turner, E. Duguet and M. Fontanille, *J. Mater. Chem.*, 1997, **7**, 1527.
34 K. S. Suslick, S. B. Choe, A. Cichowlas and M. W. Grinstaff, *Nature*, 1991, **353**, 414.
35 K. S. Suslick, T. Hyeon and M. Fang, *Chem. Mater.*, 1996, **8**, 2172.
36 C. H. Su, P. L. Wu and C. S. Yeh, *J. Phys. Chem. B*, 2003, **107**, 14 240.
37 X. Zeng, N. Koshizaki and T. Sasaki, *Appl. Phys. A: Mater. Sci. Process.*, 1999, **69**, S253.
38 B. J. Ash, R. W. Siegel and L. S. Schadler, *J. Polym. Sci., Part B: Polym. Phys.*, 2004, **42**, 4371.
39 G. Gorrasi, M. Tortora and V. Vittoria, *J. Polym. Sci., Part B: Polym. Phys.*, 2005, **43**, 2454.
40 S. Liufu, H. Xiao and Y. Li, *Polym. Degrad. Stab.*, 2004, **87**, 103.
41 S. Hsu, W. Whang, C. Hung, P. Chiang and Y. Hsiao, *Macromol. Chem. Phys.*, 2005, **206**, 291.
42 A. Bansal, H. Yang, C. Li, K. Cho, B. C. Benicewicz, S. K. Kumar and L. S. Schadler, *Nat. Mater.*, 2005, **4**, 693.
43 Y. Zhou, F. Pervin, M. Biswas, V. K. Rangari and S. Jeelani, *Mater. Lett.*, 2006, **60**, 869.
44 J. D. Rancourt and L. T. Taylor, *Macromolecules*, 1987, **20**, 790.
45 T. Sawada and S. Ando, *Chem. Mater.*, 1998, **10**, 3368.
46 P. Chiang and W. Whang, *Polymer*, 2003, **44**, 2249.
47 L. Spanhel and M. A. Anderson, *J. Am. Chem. Soc.*, 1991, **113**, 2826.
48 H. Xiong, D. Liu, Y. Xia and J. Chen, *Chem. Mater.*, 2005, **17**, 3062.
49 M. Abdullah, T. Morimoto and K. Okuyama, *Adv. Funct. Mater.*, 2003, **13**, 800.
50 Y. Li, S. Fu and Y. Mai, *Polymer*, 2006, **47**, 2127.
51 C. Hung and W. Whang, *J. Mater. Chem.*, 2005, **15**, 267.
52 H. Usui, Y. Shimizu, T. Sasaki and N. Koshizaki, *J. Phys. Chem. B*, 2005, **109**, 120.
53 H. Xiong, Z. Wang, D. Liu, J. Chen, Y. Wang and Y. Xia, *Adv. Funct. Mater.*, 2005, **15**, 1751.
54 D. Bahnemann, C. Kormann and M. R. Hoffmann, *J. Phys. Chem.*, 1987, **91**, 3789.
55 K. Vanheusden, C. H. Seager, W. L. Warren, D. R. Tallant and J. A. Voigt, *Appl. Phys. Lett.*, 1996, **68**, 403.
56 J. Antony, X. B. Chen, J. Morrison, L. Bergman, Y. Qiang, D. E. McCready and M. H. Engelhard, *Appl. Phys. Lett.*, 2005, **87**, 241 917.
57 C. L. Yang, J. N. Wang, W. K. Ge, L. Guo, S. H. Yang and D. Z. Shen, *J. Appl. Phys.*, 2001, **90**, 4489.
58 M. Demir, R. Munoz-Espi, I. Lieberwirth and G. Wegner, *J. Mater. Chem.*, 2006, **16**, 2940.
59 X. Zhang and L. C. Simon, *Macromol. Mater. Eng.*, 2005, **290**, 573.
60 S. Wu, F. Wang, C. M. Ma, W. Change, C. Kuo, H. Kuan and W. Chen, *Mater. Lett.*, 2001, **49**, 327.
61 J. Gao, B. Zhao, M. E. Itkis, E. Bekyarova, H. Hu, V. Kranak, A. Hu and R. C. Haddon, *J. Am. Chem. Soc.*, 2006, **128**, 7492.